

## Absorption spectra of perfect and imperfect Si/Ge superlattices

B. M. Adderley, R. J. Turton, and M. Jaros

*Department of Physics, The University of Newcastle Upon Tyne, Newcastle Upon Tyne, United Kingdom*

(Received 19 November 1993)

We present a comparative study of the absorption spectra for a series of systems with a 50:50 Si/Ge content. These are as follows: a random alloy, a perfect interface  $\text{Si}_5\text{Ge}_5$  superlattice, and the same superlattice with random alloy layers between the volumes of Si and Ge. It is found that the presence of any random structure reduces the peak absorption (just above the band gap) by an order of magnitude. Evidence is also given that experiment should be able to detect the difference in the absorption coefficient, between structured and random arrangements of atoms.

### I. INTRODUCTION

Recently, much theoretical<sup>1-3</sup> and experimental<sup>4-6</sup> work has been performed to investigate the properties of short period Si/Ge superlattices. This effort has been pushed by the desire to find a direct gap Si-based crystal. Such a possibility was first expressed by Gnutzman and Clausecker,<sup>7</sup> and has been confirmed from other sources.<sup>2,8</sup> As is usually the case, initial theoretical development has been based on ideal structures.<sup>9,10</sup> This is a situation that is never observed in real structures.<sup>11,12</sup> Given that the individual layers of the superlattice are themselves only a few monolayers thick, even a small degree of disturbance at the interface represents a substantial deviation from the ideal case. Recently, it has become apparent that the interfacial layers in some systems exhibit ordering along directions other than the growth direction.<sup>13-15</sup> The existence of either ordered or random alloy interface layers means that the perturbing potential is actually three dimensional. Consequently, changes to the band structure in the directions parallel to the interface must also be considered. Accounting for this will allow us to make a direct estimate of the effect of such an imperfection in this type of crystal. In this study, we shall investigate the effect of having alloy layers at the superlattice interfaces. The position of Si and Ge atoms in these alloy layers will be entirely random. More detail about the creation of such layers is given later.

It has also been argued that, for small period heterostructures, their effect on any external perturbation will be just that of an alloy containing the same concentrations of atom type. Thus, we perform a calculation using a structure where Si and Ge atoms are randomly placed in the lattice, but the ratio of Si to Ge atoms is kept the same as that for the superlattices. We can then use the features shown by the random alloy to discuss the differences introduced by the presence of ordered structure. What is the effect on the spectral shape and its magnitude? Can we lay down guidelines that will indicate, for materials of different structural and symmetry properties, what changes we might expect?

In general, it is difficult to determine the absorption coefficient  $\alpha$  accurately from either a theoretical or ex-

perimental source.<sup>16-18</sup> A great deal of computation time is required for theoretical calculations. The sum over wave vectors in the Brillouin zone being of particular concern. In experimental situations the spectra obtained from photoluminescence studies (etc.) suffer because they often also detect processes other than those of direct interest here. For instance, a measurement, made by Zachai *et al.*,<sup>19</sup> that was originally reported as evidence for an increased oscillator strength in a Si/Ge superlattice structure has now been shown to be a feature due to point or line defects in a buffer layer.<sup>20,21</sup>

We calculate  $\alpha$  via the imaginary part of the susceptibility  $\chi$ . A full-scale empirical pseudopotential calculation is performed to find  $\text{Im}[\chi^1]$ . This calculation gives us the bandstructure that we can use to determine both the density of states and joint density of states (proportional to  $\alpha$ ) of the materials under consideration here. It also gives us the matrix elements for optical transitions. In the case of the perfect superlattice the presence of a "one-dimensional" potential produces an allowed direct transition with an energy comparable to that of the phonon-assisted transition. The ordering of these transitions is dependent upon the distribution of strain in the system. The direct transition to the zone-folded minima being lowest for systems grown on Ge-rich substrates, while the phonon-assisted transition is lower in energy for Si-rich substrates. However, when we introduce alloy interface layers, the now "three-dimensional" potential, allows the no-phonon transition to the in-plane minima, thus relaxing the criterion that a Ge-rich substrate is essential for direct gap materials.

In this paper, we, therefore, study the effect on the electronic properties of superlattices, of the presence of random alloy layers at the interfaces between Si and Ge layers. The superlattices are grown on Si substrates and the calculation is performed at 0 K.

### II. CALCULATION DETAILS

All the data required to determine the linear susceptibility, and hence the absorption coefficient  $\alpha$ , was calculated using the empirical pseudopotential method.<sup>22</sup> In a

previous publication,<sup>23</sup> this method has been compared in detail to results from *ab initio* methods. Principally, in comparison to local density approximation calculations performed using CASTEP (Cambridge Serial Total Energy Programs), good agreement was found. Hence, we can expect that our results for the optical spectra near the band gap energy are as accurate as those found using other theoretical methods.

We have used potentials constructed in the manner of Friedel, Hybertsen, and Schluter<sup>24</sup> who have shown that the transition energies in a Si<sub>4</sub>Ge<sub>4</sub> superlattice strained to a Si substrate are in good agreement with those produced by a self-energy quasiparticle calculation (See Table IV of Ref. 24) The range of other computational calculations attempted includes tight binding,<sup>25</sup> *ab initio* pseudopotentials,<sup>26,27</sup> and linear-muffin-tin orbitals.<sup>28</sup> It is worth pointing out that the absolute magnitude of the fundamental gap remains uncertain in both the first principles and semiempirical calculations. As for the former they—with the exception of the many-body formulation which is not applicable to problems such as ours involving a large unit cell—do not predict the correct bulk gaps. In semiempirical methods such as ours one needs to know the value of the strain-induced splittings. Unfortunately, there is no source of suitable empirical data. Thus the gaps reported in semiempirical calculations vary depending on the choice of this splitting. This, in addition to the usual uncertainty of order 0.1 eV, accounts for the large variation of the predicted gaps in the literature. Our aim is, therefore, to focus on relative values (changes) in the magnitude of the fundamental gap as a function of changes in composition, order, and other parameters.

For the random alloy and imperfect interface cases, the calculation was performed using a supercell of 1000 atoms to model the crystal. At present, a cell of larger dimension than this is impractical due to the amount of computation time required. The supercell calculation is described in detail by reference.<sup>29</sup> To restrict the computation time to a minimum a number of modifications were made, but before we can examine these savings we need to briefly discuss the background to the supercell calculation.

### A. The supercell calculation

We expand the supercell wave functions  $\psi$  in terms of a complete set of eigenfunctions  $\theta_{n\mathbf{k}}$  corresponding to a suitable host material (here Si). Thus,

$$\psi = \sum_{n\mathbf{k}} A_{n\mathbf{k}} \theta_{n\mathbf{k}}, \quad (1)$$

where

$$\theta_{n\mathbf{k}} = \sum_{\mathbf{G}} a_{n\mathbf{k}}(\mathbf{G}) \exp^{i(\mathbf{k}+\mathbf{G})\cdot\mathbf{r}}, \quad (2)$$

$n$  is the band index,  $\mathbf{k}$  the wave vector, and  $\mathbf{G}$  the reciprocal lattice vector. The Schrödinger equation is

$$(H_0 + V)\theta = E\theta, \quad (3)$$

where  $H_0$  is the Hamiltonian of the host material and  $V$  the difference in potential between the supercell and the host. By substitution and suitable manipulation we arrive at the secular equation,

$$A_{n\mathbf{k}}(E_{n\mathbf{k}} - E)\delta_{nn'}\delta_{\mathbf{k}\mathbf{k}'} + \sum_{n\mathbf{k}} A_{n\mathbf{k}} \frac{1}{\Omega} \langle \mathbf{k}' + \mathbf{G}' | V | \mathbf{k} + \mathbf{G} \rangle = 0, \quad (4)$$

which we solve by matrix diagonalization. Finally, the matrix elements  $\frac{1}{\Omega} \langle \mathbf{k}' + \mathbf{G}' | V | \mathbf{k} + \mathbf{G} \rangle$  can be written<sup>29</sup>

$$\frac{1}{\Omega_{\text{SC}}} \sum_{\mathbf{G}\mathbf{G}'} a_{n'\mathbf{k}'}^*(\mathbf{G}') a_{n\mathbf{k}}(\mathbf{G}) \left[ v_s(\mathbf{g}) \sum_{\tau_s} \exp^{i\mathbf{g}\cdot\tau_s} + v_g(\mathbf{g}) \sum_{\tau_g} \exp^{i\mathbf{g}\cdot\tau_g} - v_o(\mathbf{g}) \sum_{\tau_o} \exp^{i\mathbf{g}\cdot\tau_o} \right]. \quad (5)$$

Here  $\Omega_{\text{SC}}$  is the volume of the supercell,  $v_s, v_g, v_o$  and  $\tau_s, \tau_g, \tau_o$  the potentials and positions of the Si, Ge, and host atoms, respectively, and  $\mathbf{g}$  is the superlattice reciprocal lattice vector,

$$\mathbf{g} = \mathbf{k}' - \mathbf{k} + \mathbf{G}' - \mathbf{G}. \quad (6)$$

When calculating the structure factors<sup>30</sup> of (5), a sum of exponential terms must be found. In the host material, and in planes of the supercell composed entirely of a single species of atom, the atoms are arranged in a regular grid. Correspondingly, the sums become just a simple geometric series. For the random interface superlattice the number of disturbed planes is approximately one half and we can, therefore, save a factor of about 4. The most substantial saving we can make occurs when we realize that the term in square brackets in (5) is only dependent on the difference in plane waves,  $\mathbf{G}' - \mathbf{G}$ . Thus, for any individual value of  $\mathbf{k}' - \mathbf{k}$ , it is only necessary to calculate this term for the set of different values  $\mathbf{G}' - \mathbf{G}$ . In a similar manner we only need to evaluate the square brackets at different values of  $\mathbf{k}' - \mathbf{k}$ . This saving is small because we use only 38 values for  $\mathbf{k}$ . However, an extra saving can be made by using time reversal symmetry to evaluate terms at  $\mathbf{k} - \mathbf{k}'$ . Finally, we can cut off the potential at  $|\mathbf{g}|^2=20$  (units of  $(2\pi/a)^2$ , where  $a$  is the lattice constant). Its form for both Si and Ge tends rapidly to zero for large values of  $|\mathbf{g}|$ , and is less than  $10^{-6}$  times the maximum positive potential, at this point.

### B. Expressions used to calculate $\chi$

The expression used to calculate the resonant first order electronic susceptibility is<sup>31-33</sup>

$$\chi_{\mu\alpha}^{(1)}(-\omega; \omega) = \sum_{vc} \sum_{\mathbf{k}} \frac{e^2 p_{vc}^{\mu} p_{cv}^{\alpha} (\rho_{vv} - \rho_{cc})}{\epsilon_0 V \hbar m^2 \omega^2 \Delta_{cv}} - \frac{e^2}{m \epsilon_0 V \omega^2}, \quad (7)$$

where

$$\Delta_{cv} = \hbar^{-1}(E_c - E_v) - \omega - i\gamma_{cv}, \quad (8)$$

and  $p_{vc}^\mu$  is the matrix element between valence subband  $v$  and conduction subband  $c$ , for polarization  $\mu$ .  $\rho_{vv}$  is the steady-state population of subband  $v$ ,  $V$  the volume of the crystal, and  $\omega$  the field frequency.  $\rho_{vv}$  and  $\rho_{cc}$  are given by

$$\rho_{vv} = \rho_o(v) + \frac{i|\beta|^2(\Delta_{vc}^{-1} + \Delta_{cv}^{-1})[\rho_o(v) - \rho_o(c)]}{\gamma_v \left[1 - i|\beta|^2(\Delta_{vc}^{-1} + \Delta_{cv}^{-1})\left(\frac{1}{\gamma_v} + \frac{1}{\gamma_c}\right)\right]}, \quad (9a)$$

$$\rho_{cc} = \rho_o(c) + \frac{i|\beta|^2(\Delta_{vc}^{-1} + \Delta_{cv}^{-1})[\rho_o(v) - \rho_o(c)]}{\gamma_c \left[1 - i|\beta|^2(\Delta_{vc}^{-1} + \Delta_{cv}^{-1})\left(\frac{1}{\gamma_v} + \frac{1}{\gamma_c}\right)\right]}, \quad (9b)$$

where

$$|\beta|^2 = \frac{e^2 p_{vc}^\mu p_{cv}^\alpha |E_\omega|^2}{4\hbar^2 m^2 \omega^2} \quad (10)$$

is the square of the Rabi flopping frequency and  $\rho_o(v)$  is the thermal equilibrium population of subband  $v$ . Note that  $\gamma_{cv} = \gamma_{vc}$  and  $\gamma_{cv} = \frac{1}{T_2^v}$ ,  $\gamma_v = \frac{1}{T_1^v}$ .  $T_2^v$  is the dipole lifetime, which indicates the loss of phase coherence between the eigenfunctions of bands  $v$  and  $c$ , and  $T_1^v$  the recombination time into band  $v$ .

### III. PERFECT INTERFACE $\text{Si}_5\text{Ge}_5$ SUPERLATTICE

Our first calculation is that for an idealized system in which all planes parallel to the interfaces contain only a single species of atom. We model a double period of  $\text{Si}_5\text{Ge}_5$ , i.e., 20 atoms (or 5 lattice constants) strained to a base of the same number of periods of Si. With all perfect layers the calculation at each superlattice wave vector can be performed in a few minutes, allowing us to sample a large number of such points.

#### A. Band structure and matrix elements

Figure 1 shows the band structure of our perfect superlattice.  $\Gamma$  is the zone center and  $X$ ,  $M$ , and  $P$  the points on the zone boundaries in the  $\langle 100 \rangle$ ,  $\langle 110 \rangle$ , and  $\langle 001 \rangle$  (growth) directions, respectively. All subbands shown are spin degenerate. As we shall be interested in the absorption coefficient near the band edge we restrict our sampling zone to a volume close to the superlattice Brillouin zone center. The size of the Brillouin zone is  $-0.2 \leq K_z \leq 0.2$ ,  $-1.0 \leq K_x, K_y \leq 1.0$   $2\pi/a$ . We sample over all  $K_z$ , but restrict to  $-0.2 \leq K_x, K_y \leq 0.2$ . As we shall be able to use the symmetry properties of the matrix elements in calculating  $\alpha$ , for this case, we can also restrict our sampling volume to one irreducible segment. In total we sampled  $\approx 33\,000$  random points in such a zone, which equates to  $\approx 412\,000$  points in the whole zone.

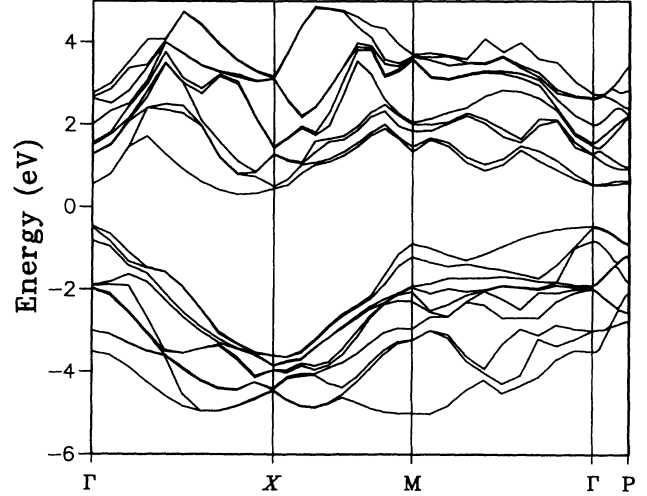


FIG. 1. Band structure of the perfect  $\text{Si}_5\text{Ge}_5$  superlattice.  $\Gamma$  is the zone center and  $X$ ,  $M$ , and  $P$  the points on the zone boundaries in the  $\langle 100 \rangle$ ,  $\langle 110 \rangle$ , and  $\langle 001 \rangle$  (growth) directions, respectively.

The energy range we investigate is from 0.7 eV to 1.5 eV. This range will cover from at least 100 meV below the threshold frequency to at least 500 meV above this value, for all the structures considered in this work. Having set this range we can use it to restrict the computation time of the absorption coefficient by cutting the number of subbands used in the calculation. It turns out that the band structure of this superlattice is such that it is only necessary to include the four uppermost valence subbands and the lowest six conduction subbands. Here

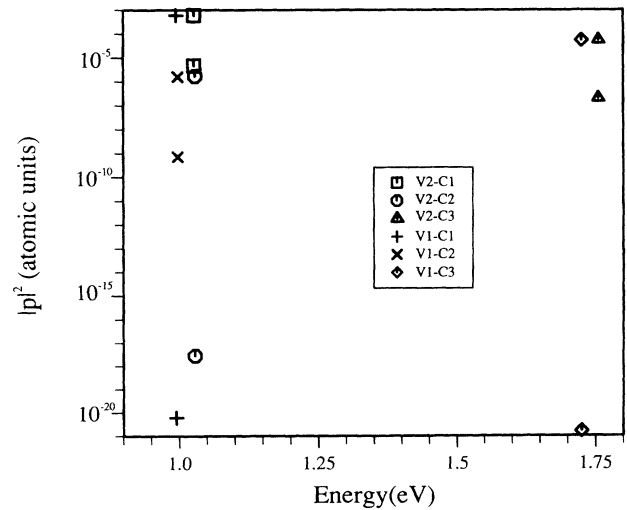


FIG. 2. The momentum matrix elements for transitions included in our calculation of  $\alpha$  at the Brillouin zone center  $\Gamma$ . V1 is the highest lying valence subband and c1 the lowest lying conduction subband. For all transitions the lower marker indicates that the z-type polarization has a weaker matrix element.

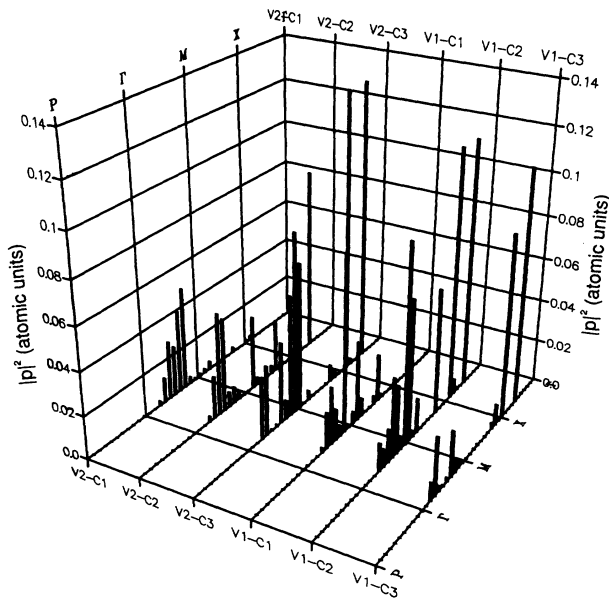


FIG. 3. The momentum matrix elements for transitions included in the calculation of  $\alpha$ . The polarization vector is  $x$ -type, and we see that in the direction of growth ( $\Gamma$  to  $P$ ), the matrix elements are small.

we have included all bands such that, at any frequency in the above range, we will be within 100 meV of resonance. Bands at energies such that we will always be at  $>100$  meV from resonance, do not contribute significantly to  $\alpha$  because of the energy denominator ( $\Delta E - \omega$ ) present in the expression for  $\chi$ .

Let us now examine, in some detail, the momentum matrix elements, Fig. 2. Here we show the values at  $\Gamma$  for

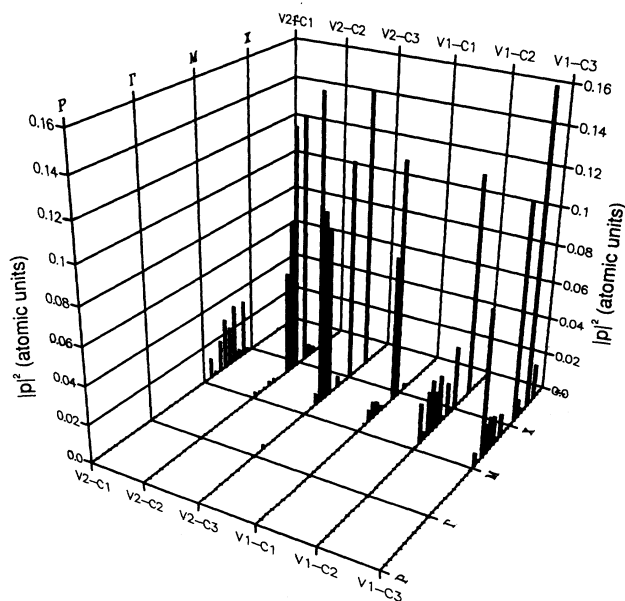


FIG. 4.  $z$ -type momentum matrix elements for the perfect superlattice, plotted against wave vector and intersubband transition. As for the  $x$ -type polarization, the matrix elements in the direction of growth are small.

transitions between subbands included in our calculation of  $\alpha$ . The (spin degenerate) bands are numbered such that  $V1$  is the highest lying (at  $\Gamma$ ) valence subband and  $C1$  the lowest lying conduction subband. In all cases the marker at a larger value of  $|p|^2$  is that for an  $x$ -type polarization, and at the lower value that for a  $z$ -type polarization. We immediately see that transitions to  $C1$  dominate at the band edge energy ( $\approx 1.0$  eV). In Fig. 3 ( $x$ -pol) and Fig. 4 ( $z$ -pol), we show the same matrix elements but at all wave vectors used to depict the band structure of Fig. 1. What is obvious is that, for both polarizations, all the matrix elements are considerably smaller in the growth ( $\Gamma$  to  $P$ ), direction. In fact, they are not discernible without the use of a logarithmic scale.

### B. The density of states

In order to calculate an accurate band structure for the superlattice it was necessary to include 20 ( $M$ ) bulk bands (4 valence and 16 conduction), and sample at 5 ( $N_{SP}$ ) points in  $k$  space (along the  $K_z$  axis). The small number of points is due to the fact that we only need include points in the bulk Brillouin zone linked to the superlattice point by a reciprocal superlattice vector. In the  $K_x$  and  $K_y$  directions the vectors are still those of the bulk material and so a shift of any one vector in these planes just returns one to a point already sampled.<sup>34</sup> Correspondingly, this gives us a total of 100 (20 valence, 80 conduction) subbands from the superlattice calculation. Using this data we calculate the density of states, Fig. 5, and the joint density of states, Figs. 6 and 7. Because we have not sampled throughout the whole of the superlattice Brillouin zone and used a restricted set of sampling points and bands, we cannot find an accurate value for the density of states, only the functional form

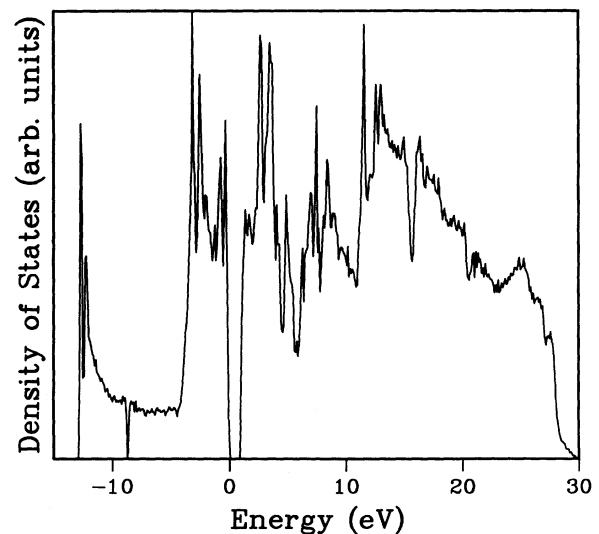


FIG. 5. The density of states for a perfect interface  $\text{Si}_5\text{Ge}_5$  superlattice grown on Si. Due to a restriction in the sampling this figure depicts only the contribution from a volume near the Brillouin zone center.

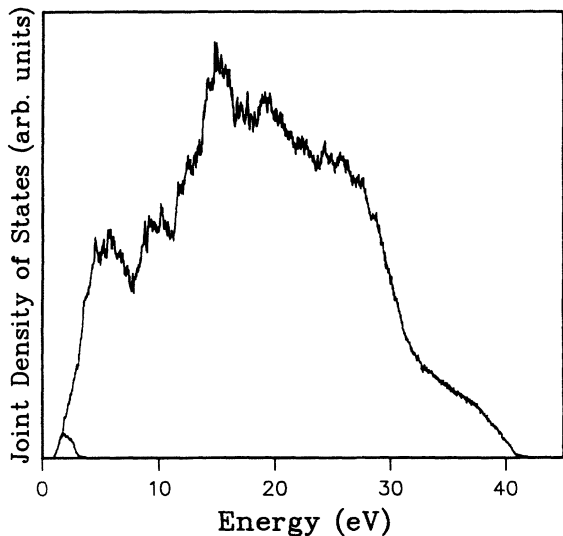


FIG. 6. The joint density of states for a perfect interface  $\text{Si}_5\text{Ge}_5$  superlattice grown on Si.

of the contribution to the density of states from the region around the zone center ( $\Gamma$ ). As the joint density of states is directly related to  $\alpha$ ,<sup>31</sup> we can use it as a guide in our calculation of  $\alpha$ . In Fig. 7, we show the joint density of states calculated using all 100 subbands, and also using only those subbands we will use in the calculation of  $\alpha$  (lower curve). We see that in the energy range we shall calculate  $\alpha$  over (0.7 eV to 1.5 eV), the two curves are almost identical. Hence we can assume that we have included all subbands necessary for the calculation of  $\alpha$ .

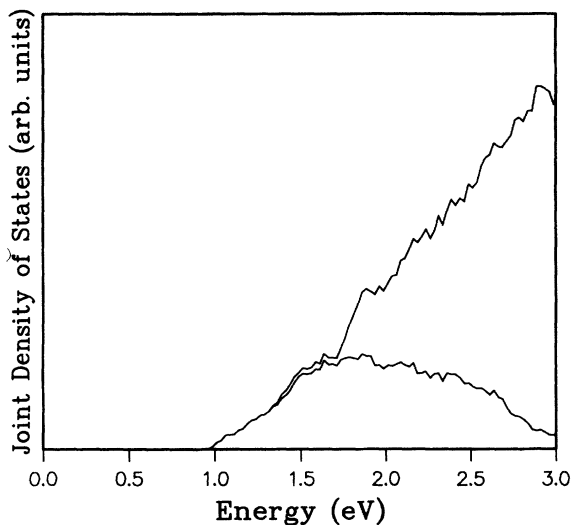


FIG. 7. Joint density of states for a perfect interface  $\text{Si}_5\text{Ge}_5$  superlattice, near the threshold energy. The lower curve is from a calculation performed using only the subbands included in the calculation of the absorption coefficient  $\alpha$ . In the energy range that we examine  $\alpha$  the full and partial calculations match.

### C. The absorption coefficient

For low field strengths the absorption coefficient  $\alpha$  is connected to the susceptibility  $\chi$  via the expression

$$\alpha_{\mu\alpha} = \frac{\omega}{n_o c} \text{Im} \left[ \chi_{\mu\alpha}^{(1)}(-\omega; \omega) \right], \quad (11)$$

where  $n_o$  is the background refractive index due to bound electrons. Using (7) and (11) we obtain Fig. 8. Here the electric field strength is set to  $1 \text{ V m}^{-1}$  and the  $\gamma$  to  $3 \text{ meV}$ .<sup>35</sup> For this structure the direct band gap energy was found to be  $0.98 \text{ eV}$  and we see that for both  $\alpha_{xx}$  (solid curve) and  $\alpha_{zz}$  (dashed curve), the onset of absorption is at this energy. The tail at lower energies for  $\alpha_{xx}$  is due to our use of a constant  $\gamma$ . Below the single photon resonance,  $\gamma$  should decrease so that  $\alpha$  tails off to zero much faster than is shown here. At energies close to the band gap it is the  $p_x$  polarization that dominates because the uppermost valence subbands are derived from the bulk heavy-hole band. Only when the energy becomes resonant with lower lying valence subbands (derived from either light-hole or split-off bands) do we see  $\alpha$  increase significantly for the  $p_z$  polarization. Note that  $\alpha_{xx} = \alpha_{yy}$  due to symmetry considerations.

### IV. IMPERFECT INTERFACE $\text{Si}_5\text{Ge}_5$ SUPERLATTICE

For this calculation we use a supercell that extends five lattice constants in the directions parallel to the interfaces and two superlattice periods, i.e., 5 times the lattice constant, along the superlattice axis. This volume contains 1000 atoms of which 400 are in the interface layers. Ideally, one would wish to use a larger supercell in order to keep periodic effects to a minimum. However,

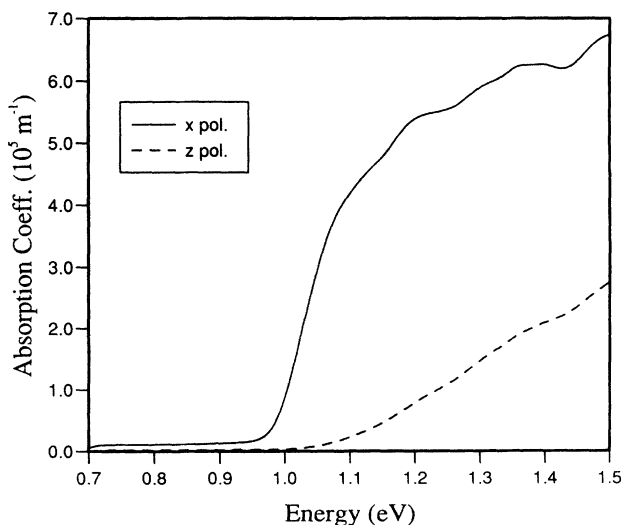


FIG. 8. The absorption coefficient  $\alpha$  for a perfect interface  $\text{Si}_5\text{Ge}_5$  superlattice (grown on Si). The band gap is  $0.98 \text{ eV}$  and  $\alpha$  increases steeply at this energy. Just above the band edge  $\alpha \approx 5 \times 10^5 \text{ m}^{-1}$ .

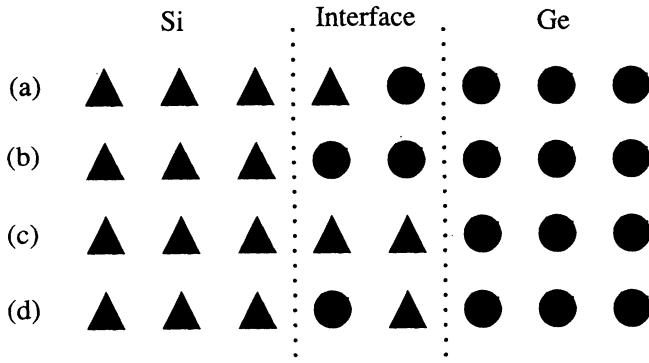


FIG. 9. Possible interface configurations. (a)–(c) are considered in this study and are as follows: (a) the ideal interface, (b) the presence of a Si atom in a Ge layer, and (c) the presence of a Ge atom in a Si layer. Configuration (d) represents “islanding” and is not included as it is taken to occur much less frequently than (a)–(c).

the amount of computation time required restricts us to a 1000 atom cell at the present time. The superlattice is strained to a Si substrate that also contains 1000 atoms.

The interface atoms are randomly assigned to be Si or Ge. By using an initialized routine we ensure that the atoms are allocated to Si or Ge, in the same order, for every superlattice  $k$  point sampled. The three interface configurations considered in this study are shown in Figs. 9(a)–9(c). Configuration (d), “islanding,” was considered to be very much less likely and was, therefore, not used.

When we examine the band structure for this material, Fig. 10, we find that the subbands are closely separated in energy and show little dispersion with wave vector throughout the Brillouin zone. This means that to cover

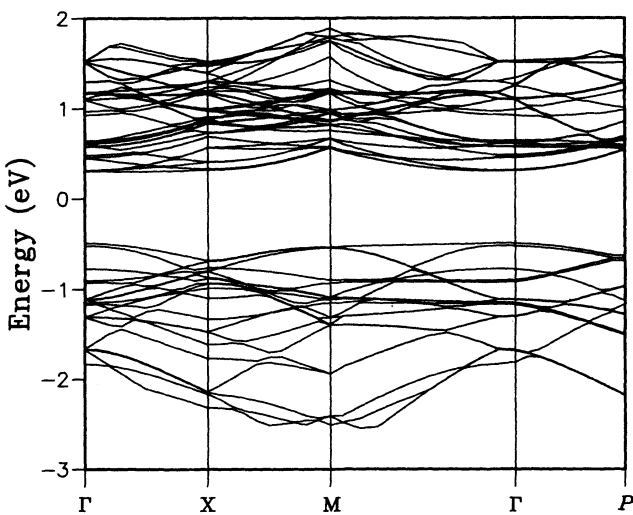


FIG. 10. Band structure of a  $\text{Si}_5\text{Ge}_5$  superlattice with randomly configured interfaces. Subbands in both the valence and conduction bands are closely spaced in energy and show little dispersion with wave vector. Consequently, we must include many subbands in the calculation of  $\alpha$  and integrate over the entire Brillouin zone.

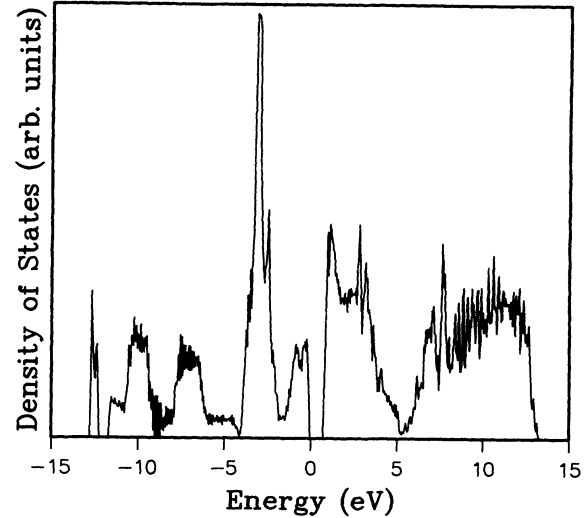


FIG. 11. Density of states for an imperfect interface  $\text{Si}_5\text{Ge}_5$  superlattice. We model 1000 atoms of the superlattice (400 of which are in the interface layers), grown on a volume of 1000 Si atoms.

the same energy range as for the perfect superlattice it is necessary to include 90 subbands (30 valence and 60 conduction) in the calculation for  $\alpha$ . We also have to sample throughout the Brillouin zone. The first reason for this is the small dispersion described above. Second, this structure does not have the symmetry properties that allow us to calculate  $\alpha$  from the sum over wave vectors in only a single irreducible segment. Unfortunately, it required three hours of computation time for each superlattice wave vector ( $M = 10, N_{\text{SP}} = 38$ ), so in total we sampled  $\approx 3200$  points.

Figure 11 shows the density of states for our imperfect interface superlattice, strained to Si. Figures 12 and 13 show the joint density of states. In Fig. 13, we see

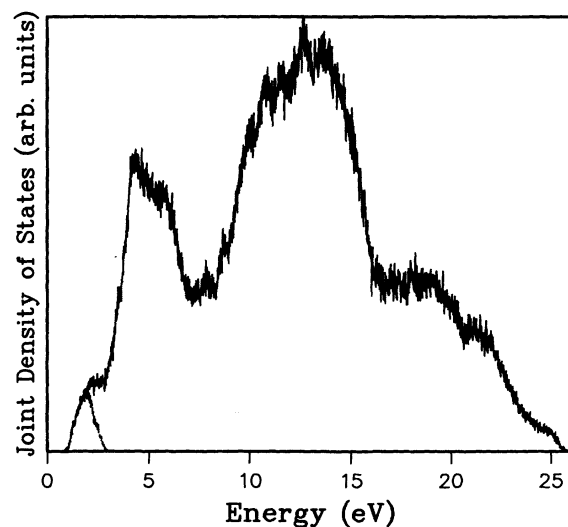


FIG. 12. Joint density of states for an imperfect interface  $\text{Si}_5\text{Ge}_5$  superlattice.

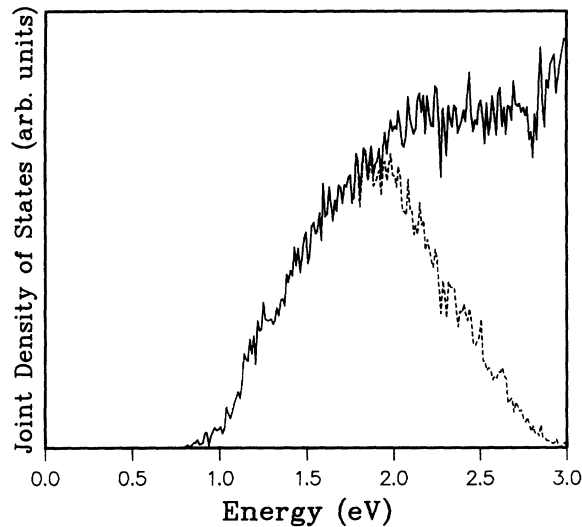


FIG. 13. Joint density of states for an imperfect superlattice, near the band gap energy. A calculation using a restricted number of subbands (dashed curve) makes no difference over the energy range in which we shall examine the absorption coefficient.

that our reduction in the sum over subbands to 90 (see above), from 380 ( $N_{SP} \times M$ ), leaves the joint density of states unchanged in the energy range we shall calculate  $\alpha$  over. Both the density of states and joint density of states for this case are very different from that of the perfect case. Obviously the reason for this is the difference in their band structure. Between these two cases the main differences are that the dispersion with wave vector is much higher in the perfect case, and that the subbands are generally much closer to each other (in energy) for the

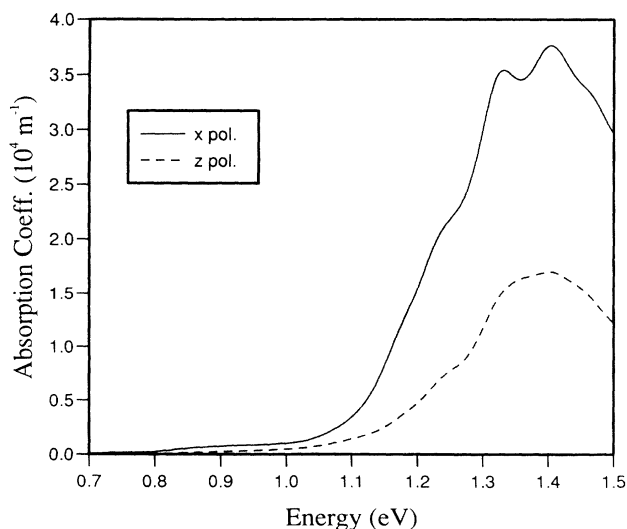


FIG. 14. The absorption coefficient  $\alpha$  of the imperfect superlattice. The magnitude has decreased by an order of 1 compared to the perfect case, due to a weakening of the zone center matrix elements.

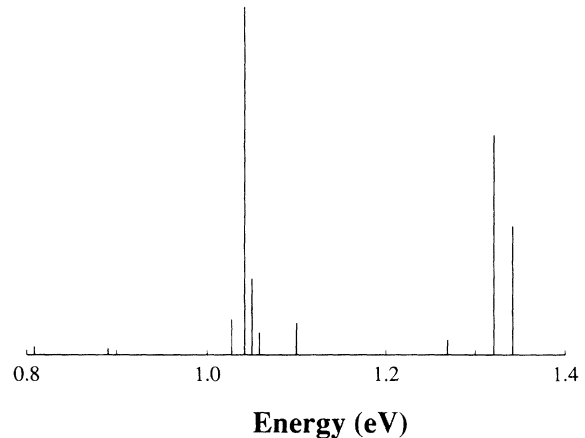


FIG. 15. Relative magnitudes of the squared optical matrix elements with  $p_x$  polarization, at the Brillouin zone center, as a function of energy for an imperfect interface  $\text{Si}_5\text{Ge}_5$  superlattice strained to a Si substrate. The transitions at lower energies are strictly forbidden in the ideal case.

imperfect case. We should also remember, and this will be a significant factor, that for the perfect superlattice we did not sample over the whole of the Brillouin zone.

The absorption coefficient is shown in Fig. 14. Immediately we see that the size of  $\alpha$  has decreased by an order of magnitude. This is because  $\alpha$ , at the absorption edge, is due to transitions at the zone center, the strength of which decreases with the amount of disorder present in the structure.<sup>23</sup> We can clearly see that the absorption is due to processes occurring in this region of the Brillouin zone by examination of Fig. 15,<sup>23</sup> which depicts the relative magnitudes of the optical matrix elements at  $\Gamma$ . Our absorption curve “envelopes” this histogram. Finally, we point out that our absorption edge and magnitude of  $\alpha$  are in good agreement with both theory<sup>9</sup> and experiment.<sup>16</sup>

## V. 50:50 Si/Ge ALLOY

Finally, we perform a calculation with a 50:50 alloy of Si and Ge, on a Si base. Both the alloy and the base volumes contain 1000 atoms, and the positions of the Si and Ge atoms in the alloy were randomly assigned. In fact, the number of Si and Ge atoms was also randomly assigned and this turned out to be 512 Ge atoms and 488 Si atoms. What we wish to achieve here is a comparison between various structures that contain the same ratio of Si and Ge atoms, i.e., under experimental conditions will it be possible to differentiate between the signals from ordered and disordered structures?

In a similar calculation to the disordered interface case we used  $M = 10$ ,  $N_{SP} = 38$  and 90 subbands in the calculation of  $\alpha$ . Again it was necessary to sample throughout the whole of the Brillouin zone, but here only 1500 sampling points were required for convergence of the sum for  $\alpha$  (in the energy range we considered). We can clearly see the reason for this by examining the band structure

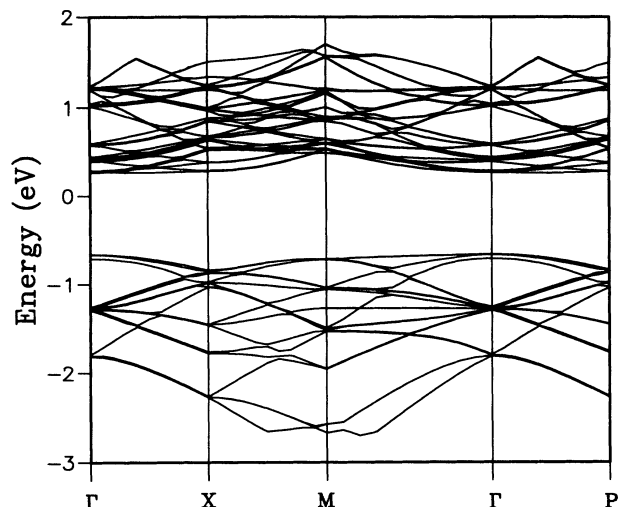


FIG. 16. Band structure of the 50:50 Si/Ge alloy. As with the random interface superlattice subbands are closely spaced in energy and show little dispersion with wave vector. Note that the structure from  $\Gamma$  to  $P$  matches that from  $\Gamma$  to  $X$ , indicating that the atoms of the alloy are in a truly random arrangement.

of the alloy, Fig. 16. Due to the truly random arrangement of atoms in the alloy the band structure is identical for  $\Gamma$  to  $P$  and  $\Gamma$  to  $X$ , i.e., the symmetry has increased. Hence, many points in one region of the Brillouin zone now also describe the response in other regions, and the sum over wave vectors correspondingly decreases.

Figure 17 shows the calculated density of states for our alloy. It is immediately apparent that this is almost identical in form to the density of states for the imperfect interface superlattice. This gives us an indication that the properties of the alloy will be very similar to those of the superlattice. Correspondingly, we would expect

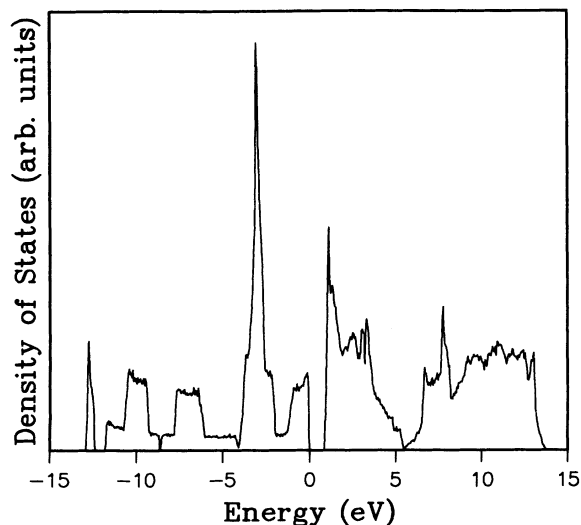


FIG. 17. 50:50 Si/Ge alloy density of states. The alloy consists of 1000 randomly arranged atoms and is strained to a volume of 1000 atoms of Si.

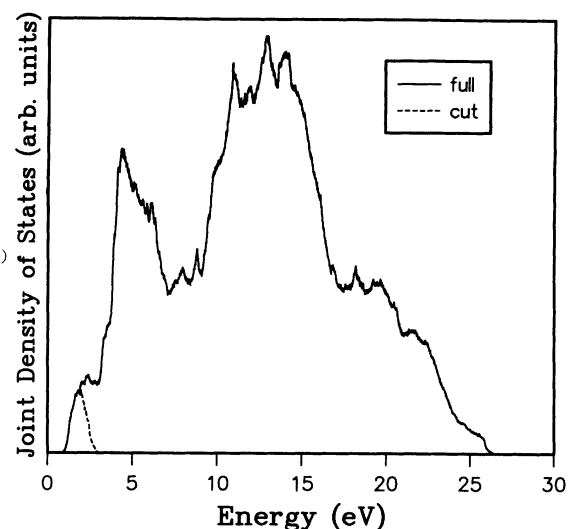


FIG. 18. Joint density of states of a 50:50 Si/Ge alloy. This closely resembles the joint density of states for the imperfect superlattice structure and we might, therefore, expect the properties of the alloy to be similar to those of the superlattice.

the joint density of states to also be very similar, Fig. 18. This is the case, and it is not until we examine a small energy range that we see the first differences, Fig. 19. In comparison to Fig. 13, the joint density of states for the alloy starts at an energy approximately 100 meV higher, i.e., the band gap of the alloy is larger. The rate of increase is also higher for the alloy at energies close to the threshold. Finally, the alloy density of states does not show the step present in Fig. 13 at  $\approx 2.75$  eV. All

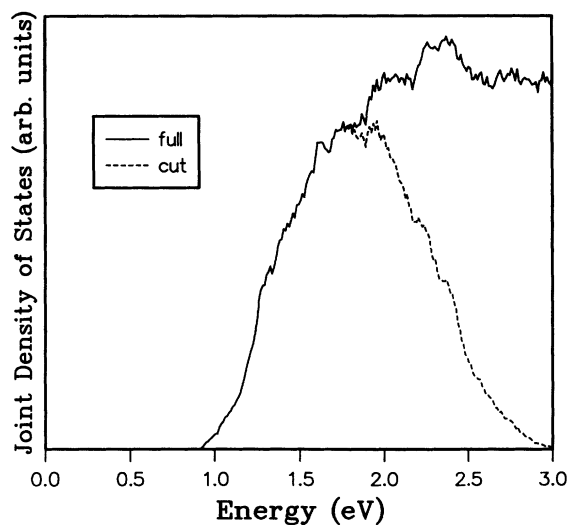


FIG. 19. A magnified view of the joint density of states for the Si/Ge alloy, close to the band gap energy. This detailed view shows up differences from the joint density of states of the imperfect superlattice and indicates that although the gross band structure may well be similar, the subband structure is somewhat different.

these features indicate that although the gross structure of the alloy and superlattice may be similar, the subband structure is somewhat different. This would show itself in more detail if one could examine the nonlinear absorption (via  $\chi^{(3)}$ , etc.).<sup>36</sup>

How does the absorption coefficient in the alloy (Fig. 20), compare to that of the imperfect interface superlattice? The first thing to state is that the alloy has no regular structure. This should mean that  $\alpha$  is the same for all polarizations, which it is found to be (within the convergence limit of our calculation). The band gap of the alloy is 0.92 eV, and  $\alpha$  picks up steeply at this energy. Unlike the imperfect superlattice the transition probabilities across the band gap are the same order of magnitude as those at the in plane minima, so that there is no "ledge" at lower energies. In overall magnitude the alloy absorption coefficient is an order of magnitude less than that for the perfect superlattice, but larger than that for the imperfect case. Compared to the perfect superlattice the matrix elements at the zone center are small (cf. the imperfect superlattice), but larger at the in plane minima than those of the random interface.

We also plot the ratio  $\alpha_{\text{int}}/\alpha_{\text{alloy}}$ . By doing this we hope to pick out features that an experiment could detect. The most prominent feature of Fig. 21 is undoubtedly the peak at  $\approx 0.86$  eV, which occurs for both  $p_x$  and  $p_z$  polarizations. The peak is created by the nonzero matrix elements for the zone center (band gap), transition in the random interface case. The alloy has no states below 0.92 eV so any absorption is just from the tail of the absorption edge. In any experiment, probably the easiest confirmation of the effect of an ordered structure would be the fact that the ratio  $\leq 0.5$  for all energies and a  $p_z$  polarization. This ratio should always be equal to 1 for any experiment that can detect no difference be-

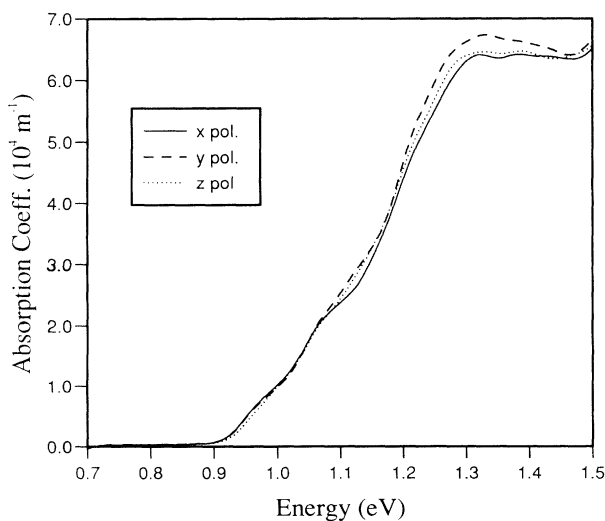


FIG. 20. Absorption coefficient for the 50:50 Si/Ge alloy. The structure is shown to be truly random by  $\alpha$  being the same for all polarizations. The peak value away from the band edge ( $\approx 6 \times 10^4 \text{ m}^{-1}$ ), is larger than that for the imperfect superlattice because the matrix elements at the in-plane minima are stronger.

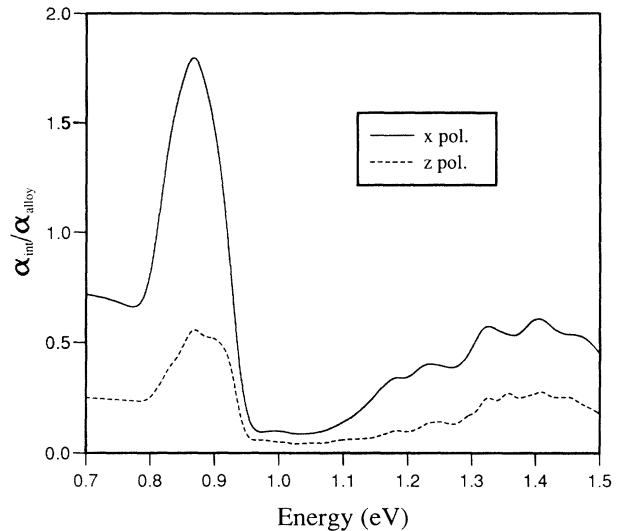


FIG. 21. The ratio of the absorption coefficients for the imperfect superlattice and the random alloy. The superlattice has allowed transitions (though small in magnitude) at its direct gap, creating the peak(s) at  $\approx 0.86$  eV. If experiments were unable to detect the difference between the structured and random materials the ratio should be 1 at all energies.

tween structured and random materials containing the same (small) numbers of Si and Ge atoms.

## VI. CONCLUSIONS

In this work, we set out to investigate the effect of interface disorder on the absorption coefficient  $\alpha$  shown by a  $\text{Si}_5\text{Ge}_5$  superlattice (on a Si base). We were able to demonstrate that the dominant effect is a decrease of an order of magnitude in  $\alpha$ , due to the weakening of the direct band gap matrix elements. Close to the band edge  $\alpha$  for the perfect superlattice was found to be  $\approx 6 \times 10^5 \text{ m}^{-1}$  ( $x$ -pol), and  $\approx 3 \times 10^5 \text{ m}^{-1}$  ( $z$ -pol). For the random interface superlattice we find  $\approx 3 \times 10^4 \text{ m}^{-1}$  ( $x$ -pol) and  $\approx 2 \times 10^4 \text{ m}^{-1}$  ( $z$ -pol). The respective threshold energies are 0.98 eV and 0.80 eV.

We then proceeded with a calculation for a completely random alloy containing the same total number and ratio of Si and Ge atoms as the superlattices. This structure is used to discuss the differences created in the absorption spectra, by the introduction of ordering.  $\alpha$  for the alloy was found to be of the same order as that of the imperfect interface superlattice, but detailed investigation showed up features suitable for experimental investigation. The most simple difference is that the loss of symmetry, when moving from the alloy to the superlattice, results in a significantly different magnitude of response for polarizations parallel and perpendicular to the direction of growth of the superlattice, in this case, at least a factor of 2 for all the frequencies in the range we investigated. The other significant factors found in our study

are that the absorption edge is approximately 100 meV higher in energy for the alloy than the disordered interface superlattice, and that unlike the imperfect superlattice the transition probabilities across the band gap (for the alloy) are the same order of magnitude as those at the in-plane minima. For the superlattice this last point means that the absorption coefficient remains very low until we reach an energy approximately 300 meV above the band edge. We, therefore, predict that experiment should be able to verify the effect on  $\alpha$  of having an ordered structure.

Using the data needed to calculate  $\alpha$  we were also able to present calculations of the density of states, and joint

density of states (proportional to  $\alpha$ ) for all the structures considered in this study.

#### ACKNOWLEDGMENTS

This work has been supported by the ESPRIT European basic research program, the Science and Engineering Research Council (UK), and the Office of Naval Research (USA). We are grateful to the Theory of Condensed Matter Group, Cambridge University, UK, for making available the suite of programs for performing total energy calculations.

- <sup>1</sup> M. A. Gell, Appl. Phys. Lett. **55**, 484 (1989).
- <sup>2</sup> R. J. Turton and M. Jaros, Mater. Sci. Eng. B **7**, 37 (1990).
- <sup>3</sup> C. Tserbak, H. M. Polatoglou, and G. Theodorou, Europhys. Lett. **18**, 451 (1992).
- <sup>4</sup> F. Cerdeira, M. I. Alonso, D. Nilas, M. Garriga, M. Cardona, E. Casper, and H. Kibbel, Phys. Rev. B **40**, 1361 (1991).
- <sup>5</sup> Y. Yin, D. Yan, F. H. Pollack, M. S. Hybertsen, J. M. Vandenberg, and J. C. Bean, Phys. Rev. B **44**, 5955 (1991).
- <sup>6</sup> U. Schmid, J. Humlicek, F. Lukes, M. Cardona, H. Presting, H. Kibbel, E. Kasper, K. Eberl, W. Wegscheider, and G. Abstreiter, Phys. Rev. B **45**, 6793 (1992).
- <sup>7</sup> U. Gnuzman and K. Clausecker, Appl. Phys. **3**, 9 (1974).
- <sup>8</sup> T. P. Pearsall, CRC Crit. Rev. Solid State Mater. Sci. **15**, 551 (1989).
- <sup>9</sup> H. M. Polatoglou, Phys. Rev. B (to be published).
- <sup>10</sup> M. A. Gell and A. C. Churchill, Phys. Rev. B **39**, 10 449 (1989).
- <sup>11</sup> K. Eberl, G. Krotz, R. Zachai, and G. Abstreiter, J. Phys. (Paris) Colloq. **48**, C5-329 (1987).
- <sup>12</sup> T. P. Pearsall, J. Bevk, J. C. Bean, J. Bonar, J. P. Mannaerts, and A. Ourmazd, Phys. Rev. B **39**, 3741 (1989).
- <sup>13</sup> D. E. Jesson, S. J. Pennycook, and J.-M. Baribeau, Phys. Rev. Lett. **66**, 750 (1991).
- <sup>14</sup> D. E. Jesson, S. J. Pennycook, J.-M. Baribeau, and D. C. Houghton, Phys. Rev. Lett. **68**, 2062 (1992).
- <sup>15</sup> E. Muller, H.-U. Nissen, M. Ospelt, and H. von Kanel, Phys. Rev. Lett. **63**, 1819 (1989).
- <sup>16</sup> J. Olajos, J. Engvall, H. G. Grimmeiss, U. Menczigar, G. Abstreiter, J. Kibbel, E. Kasper, and H. Presting, Phys. Rev. B **46**, 12 857 (1992).
- <sup>17</sup> P. K. Basu and S. K. Paul, Phys. Rev. B **46**, 13 389 (1992).
- <sup>18</sup> A. A. Chowdhury, M. M. Rashed, C. M. Maziar, S. S. Murtaza, and J. C. Campbell, J. Vac. Sci. Technol. B **11**, 1685 (1993).
- <sup>19</sup> R. Zachai, K. Eberl, G. Abstreiter, E. Kasper, and H. Kibbel, Phys. Rev. Lett. **64**, 1055 (1990).
- <sup>20</sup> K. Terashima, M. Tajima, and T. Tatsumi, Appl. Phys. Lett. **57**, 1925 (1990).
- <sup>21</sup> J. -P. Noel, N. L. Rowell, D. C. Houghton, and D. D. Perovic, Appl. Phys. Lett. **57**, 1037 (1990).
- <sup>22</sup> M. Jaros and K. B. Wong, J. Phys. C **17**, L765 (1984).
- <sup>23</sup> R. J. Turton and M. Jaros, Semi. Cond. Sci. Tech. **8**, 2003 (1989).
- <sup>24</sup> P. Friedel, M. S. Hybertsen, and M. Schluter, Phys. Rev. B **39**, 7974 (1989).
- <sup>25</sup> L. Brey and C. Tejeder, Phys. Rev. Lett. **59**, 1022 (1987).
- <sup>26</sup> S. Froyen, D. M. Wood, and A. Zunger, Phys. Rev. B **37**, 6893 (1987).
- <sup>27</sup> M. S. Hybertsen and M. Schluter, Phys. Rev. B **36**, 9683 (1987).
- <sup>28</sup> U. Schmid, N. E. Christenson, M. Alouani, and M. Cardona, Phys. Rev. B **43**, 14 597 (1991).
- <sup>29</sup> I. Morrison, M. Jaros, and K. B. Wong, Phys. Rev. B **35**, 9693 (1987).
- <sup>30</sup> M. L. Cohen and T. K. Bergstresser, Phys. Rev. **141**, 789 (1966).
- <sup>31</sup> P. N. Butcher and D. Cotter, *The Elements of Nonlinear Optics* (Cambridge University Press, Cambridge, England, 1990).
- <sup>32</sup> B. S. Wherrett and N. A. Higgins, Proc. R. Soc. London, Ser. A **379**, 67 (1982).
- <sup>33</sup> C. Flytzanis, in *Quantum Electronics*, edited by H. Rabin and C. L. Tang (Academic, New York, 1975), Vol. 1A, p. 154.
- <sup>34</sup> M. A. Gell, Ph.D. thesis, University of Newcastle Upon Tyne, UK, 1986.
- <sup>35</sup> I. Morrison and M. Jaros, Phys. Rev. B **42**, 3749 (1990).
- <sup>36</sup> M. Shaw, D. Ninno, B. M. Adderley, and M. Jaros, Phys. Rev. B **45**, 11 031 (1992).